Search for Lorentz violation in short-range gravity

J. C. Long and V. Alan Kostelecký

Search for Lorentz violation in short-range gravity

J.C. Long and V. Alan Kostelecký

Physics Department, Indiana University, Bloomington, IN 47405, U.S.A.

A search for sidereal variations in the force between two planar tungsten oscillators separated by about 80 μm sets the first experimental limits on Lorentz violation involving quadratic couplings of the Riemann curvature, consistent with no effect at the level of 10^{-7} m^2.

FIG. 1: Schematic of the Indiana short-range experiment.

Local Lorentz invariance is a foundational component of General Relativity (GR), which currently remains our most successful theory of gravity. However, GR is formulated as a classical theory, and merging it with quantum physics in a consistent manner may well demand changes in its foundational structure. Even if local Lorentz invariance is exact in the underlying theory of quantum gravity, spontaneous breaking of this symmetry may occur, leading to tiny observable effects [1]. Experimental studies of Lorentz invariance are therefore valuable as probes of the foundations of GR.

Short-range experiments are uniquely sensitive probes of gravity at scales below about a millimeter and hence offer interesting opportunities to search for new physics beyond GR [2]. The essence of short-range experiments is to measure the force between two masses separated by a small distance. To attain sensitivity at short range without being overwhelmed by Newton forces at larger scales, the test masses are typically scaled to that range. Experiments of this type are well suited, for example, to searching for deviations from the gravitational inverse-square law.

To date, most studies of local Lorentz invariance in gravity are restricted to matter-gravity couplings [3, 4]. However, recent theoretical work [5] using effective gravitational field theory [6] shows that quadratic curvature couplings involving Lorentz violation lead to interesting new effects in short-range experiments that could have escaped detection in conventional studies to date. The Poisson equation for the Newton gravitational potential $U(\boldsymbol{r})$ generated by a source of mass density $\rho(\boldsymbol{r})$ acquires an extra perturbative term with four spatial derivatives,

$$-\vec{\nabla}^2 U = 4\pi G_N \rho + (\overline{k}_{\text{eff}})_{jklm}\partial_j\partial_k\partial_l\partial_m U, \qquad (1)$$

where $(\overline{k}_{\text{eff}})_{jklm}$ are effective coefficients with dimensions of squared length that can be taken as constant on the scale of the solar system [7]. The extra term violates rotation symmetry and hence Lorentz invariance. It is the general leading-order term in a natural perturbative expansion because a term with three derivatives is excluded by Newton's third law [5]. The presence of four derivatives implies corrections to the Newton force that are inverse quartic and hence appear only at short range. The rotation violation implies effects in the laboratory depending on orientation and also on sidereal time due to the rotation of the Earth, thereby ensuring that the resulting experimental signals are distinct from those associated with conventional Yukawa or inverse-power correcti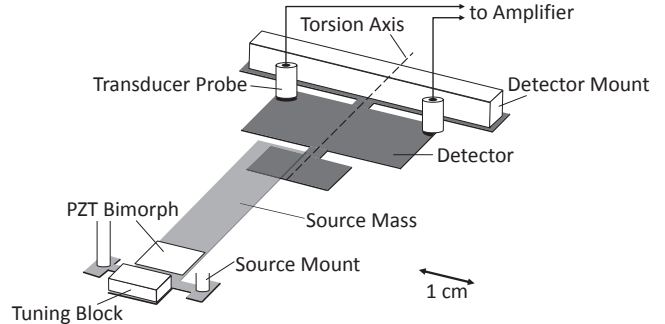ons. The extra term offers a general description of the dominant noncentral short-range corrections to Newton gravity arising from an underlying unified theory.

Here, we present new data acquired in March 2012 from a short-range experiment [8–10] located in Bloomington, IN. We use these data to search for sidereal variations involving noncentral inverse-quartic corrections to Newton's law, obtaining first constraints on quadratic Lorentz-violating curvature couplings at the level of 10^{-7} m^2. We also extend the analysis to incorporate the 2002 dataset obtained with the apparatus located in Boulder, CO [9]. Note that existing searches for pure-gravity local Lorentz violation within this framework have been restricted to the context of a Lorentz-violating inverse-*square* law [11–18]. A few other short-range experiments [19–22] may have potential sensitivity to the modifications (1), while some experiments optimized for nonperturbative corrections to Newton's law could conceivably be adjusted to study perturbative effects [23–26]. Note also that constraints on forces with various inverse-power laws have appeared in the literature [27], but only in the context of Lorentz-invariant effects.

The design and operation of the experiment is described elsewhere [8–10]. Here, we summarize briefly the basic features. Each of the two test masses is a planar tungsten oscillator of approximate thickness 250 μm, separated by a gap of about 80 μm, arranged as shown in Fig. 1. A stiff conducting shield is placed between them to suppress electrostatic and acoustic backgrounds. The planar geometry concentrates as much mass as possible at the scale of interest while being nominally null with respect to inverse-square forces, thereby suppressing the Newton background relative to new short-range effects. The force-sensitive 'detector' mass is driven by the force-generating 'source' mass at a resonance near 1 kHz. Vi-

bration isolation is a key requirement for this setup, and operation at 1 kHz is chosen because at this frequency a comparatively simple passive vibration-isolation system can be used. The entire apparatus is enclosed in a vacuum chamber and operated at 10^{-7} torr to minimize the acoustic coupling. Detector oscillations are read out via capacitive transducer probes coupled to a sensitive differential amplifier, with the signal fed to a lock-in amplifier referenced by the same waveform used to drive the source mass. This design has proved effective in suppressing all background forces to the extent that only thermal noise is observed, arising from dissipation in the detector mass. The output of the lock-in amplifier constitutes the raw data. These data are converted to force readings by comparison with the detector thermal noise, the scale of which is determined using the equipartition theorem [8]. Following data collection in 2002, this experiment set the strongest limits on unobserved forces of nature between 10 and 100 μm [9]. The apparatus has since been optimized to explore gaps below 50 μm, and operation at the thermal noise limit has recently been demonstrated [10].

Measuring the coefficients $(\overline{k}_{\text{eff}})_{jklm}$ in Eq. (1) is the goal of the present analysis. The coefficients are totally symmetric, implying 15 independent observables for Lorentz violation. Following standard convention, we extract values of these observables in the canonical Sun-centered frame [3, 28], with Z axis along the direction of the Earth's rotation and X axis pointing towards the vernal equinox. As the Earth rotates, the coefficients measured in the laboratory vary with sidereal time T. The Earth's boost $\beta_\oplus \simeq 10^{-4}$ can be neglected here. The transformation from the Sun-centered frame (X, Y, Z) to the laboratory frame (x, y, z) therefore involves a time-dependent rotation $R^{jJ}(T)$ [5] that depends on the Earth's sidereal frequency $\omega_\oplus \simeq 2\pi/(23 \text{ h } 56 \text{ min})$ and the colatitude χ of the laboratory, which is 0.887 in Bloomington and 0.872 in Boulder. The laboratory coefficients $(\overline{k}_{\text{eff}})_{jklm}(T)$ are thus related to the coefficients $(\overline{k}_{\text{eff}})_{JKLM}$ in the Sun-centered frame by

$$(\overline{k}_{\text{eff}})_{jklm}(T) = R^{jJ}R^{kK}R^{lL}R^{mM}(\overline{k}_{\text{eff}})_{JKLM}. \quad (2)$$

The cartesian components $g^j(\boldsymbol{r}, T)$ of the modified gravitational acceleration at position $\boldsymbol{r}$ and at sidereal time T contain the conventional Newton acceleration along with an inverse-quartic correction term,

$$g^j(\boldsymbol{r}, T) = -G_N \int d^3r' \rho(\boldsymbol{r}') \left(\frac{\widehat{R}^j}{|\boldsymbol{r} - \boldsymbol{r}'|^2} + \frac{\overline{k}^j(\widehat{\boldsymbol{R}}, T)}{|\boldsymbol{r} - \boldsymbol{r}'|^4} \right). \quad (3)$$

Here, $\widehat{\boldsymbol{R}} = (\boldsymbol{r} - \boldsymbol{r}')/|\boldsymbol{r} - \boldsymbol{r}'|$, while

$$\begin{aligned} \overline{k}^j(\widehat{\boldsymbol{R}}, T) = {}& \tfrac{105}{2}(\overline{k}_{\text{eff}})_{klmn}\hat{R}^j\hat{R}^k\hat{R}^l\hat{R}^m\hat{R}^n \\ & -45(\overline{k}_{\text{eff}})_{klmm}\hat{R}^j\hat{R}^k\hat{R}^l + \tfrac{9}{2}(\overline{k}_{\text{eff}})_{klkl}\hat{R}^j \\ & -30(\overline{k}_{\text{eff}})_{jklm}\hat{R}^k\hat{R}^l\hat{R}^m + 18(\overline{k}_{\text{eff}})_{jkll}\hat{R}^k \quad (4) \end{aligned}$$

controls the inverse-quartic force correction, which varies with direction $\widehat{\boldsymbol{R}}$ and sidereal time T. Note that the T

dependence is oscillatory and includes components up to the fourth harmonic of $\omega_\oplus$.

The detector is a constrained mechanical oscillator with distributed mass. The modal amplitude at any point in the detector mass is strongly dominated by vertical motion. This is particularly true near the thermal noise limit, where the amplitudes are of order 1 pm [10]. The experiment is thus sensitive predominantly to the z component F_p of the effective force at the location of the capacitive probe, which can be written as

$$F_p(T) = \frac{1}{d} \int_D d^3r \, \xi(\boldsymbol{r}) F^z(\boldsymbol{r}, T). \quad (5)$$

Here, $\xi(\boldsymbol{r})$ is the detector mode-shape function, which is the amplitude of the displacement of the detector at point $\boldsymbol{r}$ when undergoing free oscillations in the relevant mode of interest, and the displacement d is the oscillation amplitude of the detector at the location of the probe. These quantities are derived from a finite-element model of the detector mass and have the same arbitrary normalization. The integration is taken over the volume D of the detector over which the force is applied.

For the purposes of the present analysis, Eq. (5) is evaluated by Monte-Carlo integration, using the z component $F^z(\boldsymbol{r})$ of the force (3) expressed in terms of the coefficients $(\overline{k}_{\text{eff}})_{JKLM}$ in the Sun-centered frame along with the geometrical parameters listed in Table II of Ref. [8]. Note that the source amplitude for the 2012 dataset was 22.2 ± 3.2 μm and the average gap was 77.5 ± 20 μm. The experiment is performed on resonance, so the Monte-Carlo algorithm computes the Fourier amplitude of Eq. (5) averaged over a complete cycle of the source-mass oscillation, taking into account the measured source-mass curvature and mode shape. The result can be expressed as a Fourier series in the sidereal time T,

$$F_p(T) = \tfrac{1}{2}C_0 + \sum_{m=1}^{4} S_{m\omega}\sin(m\omega_\oplus T) + C_{m\omega}\cos(m\omega_\oplus T). \quad (6)$$

The Fourier amplitudes in this expression are linear combinations of the coefficients $(\overline{k}_{\text{eff}})_{JKLM}$. Their weights are functions of the source and detector mass geometry and the laboratory colatitude. Using approximately 500 million random pairs of points for each test mass suffices to resolve all harmonics. Systematic errors from the dimensions and positions of the test masses [8] can be determined at this stage, by computing the mean and standard deviation of a population of Fourier amplitudes generated with a spread of geometries based on metrology errors. For the 2002 data, the systematic error on the weights ranges from about 10% to 75%. For the 2012 data, it ranges from 15% to 50% on the most resolvable terms, while a few poorly resolved ones have systematic errors in excess of 100%. Most of the systematic error is due to the uncertainty in the average gap, with a smaller contribution from the source amplitude.

All 15 independent components of $(\overline{k}_{\text{eff}})_{JKLM}$ appear in the Fourier series (6), although no single amplitude
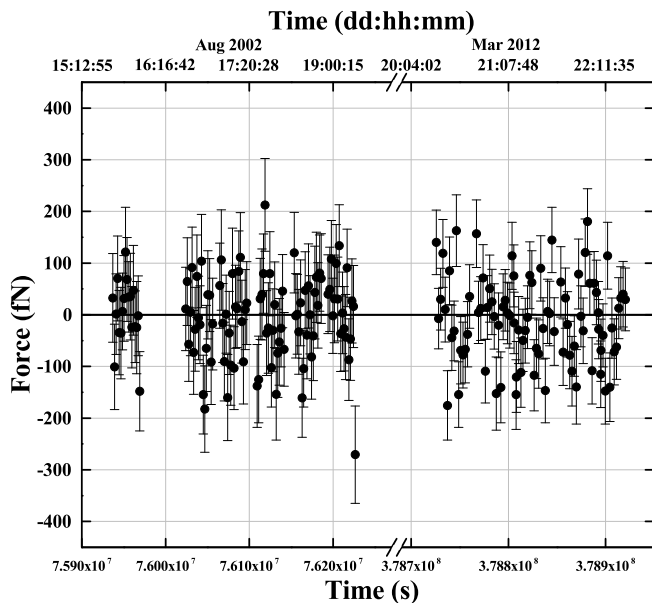
FIG. 2: Data from the Indiana short-range experiment.

	2012 data	2012 data	2002 data	2002 data
Mode	$\tilde{d}_k$	$\tilde{D}_k$	$\tilde{d}_k$	$\tilde{D}_k$
C_0	-8.1 ± 5.0	-3.1 ± 6.2	-4.2 ± 7.8	1.7 ± 19.1
S_ω	-0.7 ± 6.8	-2.9 ± 8.7	24.9 ± 9.6	14.4 ± 22.9
C_ω	7.5 ± 7.3	7.2 ± 7.8	-2.2 ± 12.2	-2.6 ± 11.5
$S_{2\omega}$	-4.1 ± 7.1	-10.1 ± 8.7	-16.9 ± 12.0	-4.3 ± 12.4
$C_{2\omega}$	-9.4 ± 7.0	-11.3 ± 7.6	-0.8 ± 9.9	-11.0 ± 26.4
$S_{3\omega}$	-17.2 ± 7.1	-18.9 ± 7.4	33.5 ± 10.4	30.8 ± 20.8
$C_{3\omega}$	-11.8 ± 7.0	-15.6 ± 8.9	-19.2 ± 11.5	-17.5 ± 12.6
$S_{4\omega}$	-0.9 ± 7.1	0.1 ± 7.6	0.6 ± 11.3	6.7 ± 13.8
$C_{4\omega}$	3.4 ± 7.1	-1.1 ± 8.1	9.1 ± 10.7	8.8 ± 21.7

TABLE I: Fourier transforms in fN units.

contains all of them. The transformation (2) predicts some simple relations among the amplitudes, each of which is satisfied by the results of the numerical integration. Performing the numerical integration for a hypothetical geometry with an average gap an order of magnitude larger than the largest dimension of either mass produces a result agreeing to within a few percent with the analytical expression for point masses of the same mass and separation. This limiting case confirms that some contributions from $(\overline{k}_{\text{eff}})_{JKLM}$ are resolvable only due to the planar geometry.

Figure 2 displays the force data acquired during the runs in 2012 and in 2002 as a function of the sidereal time T measured in seconds from $T = 0$, which is taken to be the 2000 vernal equinox. The force data were collected at a 1 Hz rate in 14.4-minute sets (2012 run) and in 12-minute sets (2002 run), with comparable intervals between each set during which diagnostic data were taken to monitor the experiment for gain and frequency drifts. Each data point represents the mean of a 14.4- or 12-minute set. Each error bar shown is the 1σ standard deviation of the mean, including both the statistical uncertainty and the systematic errors associated with the force calibration. The 2002 force calibration and parameters are given by Eq. (2) and Table 1 of Ref. [8]. The 2012 parameters are unchanged except that the mechanical quality factor was 22479 ± 64, the resonance frequency was 1191.32 ± 0.015 Hz, and the integrated mode shape was $(6.0 \pm 0.6) \times 10^{-11}$ m$^{5/2}$. The calibration uncertainties for the 2002 and 2012 data increase the errors by about 1% and 2%, respectively.

Figure 2 represents a finite time series of force data with uneven time distribution. To analyze the data for Lorentz violation, we adopt a well-established procedure [13]. The ideal measure of each harmonic signal component is the corresponding Fourier amplitude in Eq. (6). Each of these nine amplitudes, $k = 1, \ldots 9$, can be estimated by the discrete Fourier transform $\tilde{d}_k = \frac{2}{N} \sum_j f(T_j) a_k(T_j)$, where N is the total number of force-data points plotted in Fig. 2, $f(T_j)$ are the values of the force at each time T_j, and $a_k(T_j)$ is either $\sin(\omega_k T_j)$ or $\cos(\omega_k T_j)$ with $\omega_k = m\omega_\oplus$, $m = 0, 1, 2, 3, 4$. For this part of the analysis, we treat the 2012 and 2002 results as separate datasets. The nine components $\tilde{d}_k$ extracted from the 2012 dataset and from the 2002 dataset are listed in the second and fourth columns of Table I. The uncertainties are determined by propagating the errors of the time-series data in Fig. 2. The uncertainties can also be estimated by computing the Fourier transforms at several frequencies above and below the signal frequency and calculating the root mean square of the values obtained. The former method is slightly more pessimistic and is adopted here.

For a finite time series, the Fourier components overlap. The overlap can be quantified by a correlation covariance matrix $\text{cov}(a_k, a_{k'}) = (2/N) \sum_j a_k(T_j) a_{k'}(T_j)$. The covariance matrix relates the amplitudes $\tilde{D}_k$ for continuous data to the amplitudes $\tilde{d}_k$ for discrete data according to $\tilde{d}_k = \sum_{k'} \text{cov}(a_k, a_{k'}) \tilde{D}_{k'}$. The nine continuous amplitudes $\tilde{D}_k$ can be obtained by applying the inverse matrix cov^{-1}. For the 2012 and 2002 datasets, the results of this calculation are also displayed in the third and fifth columns of Table I. The $\tilde{D}_k$ can be taken to represent the measured values of the force components. These values largely are consistent with zero within the quoted errors, which include the small calibration systematics along with statistical errors. The modes at 3ω appear to display resolved signals at this stage. However, the associated coefficient weights are tiny, so these force components become swamped by position systematics in the final results below.

Individual measurements of the independent components of $(\overline{k}_{\text{eff}})_{JKLM}$ can be extracted from a global probability distribution formed using the values of the nine continuous amplitudes $\tilde{D}_k$ and their errors. Each measured amplitude can be assigned a corresponding proba-

Coefficient	2012 value $(10^{-7}\ \mathrm{m}^2)$	2002 value $(10^{-7}\ \mathrm{m}^2)$	Combined $(10^{-7}\ \mathrm{m}^2)$
$(\overline{k}_{\mathrm{eff}})_{XXXX}$	1.1 ± 3.2	0.5 ± 16.1	1.1 ± 3.1
$(\overline{k}_{\mathrm{eff}})_{YYYY}$	0.5 ± 3.2	-1.7 ± 16.2	0.4 ± 3.1
$(\overline{k}_{\mathrm{eff}})_{ZZZZ}$	0.6 ± 2.5	-0.7 ± 14.9	0.6 ± 2.5
$(\overline{k}_{\mathrm{eff}})_{XXXY}$	5.3 ± 19.5	2.5 ± 34.9	-3.4 ± 15.8
$(\overline{k}_{\mathrm{eff}})_{XXXZ}$	-9.5 ± 13.7	-5.9 ± 28.7	-8.1 ± 10.7
$(\overline{k}_{\mathrm{eff}})_{YYYX}$	-5.7 ± 19.5	-1.0 ± 35.1	-4.4 ± 15.8
$(\overline{k}_{\mathrm{eff}})_{YYYZ}$	7.3 ± 12.2	-31.7 ± 44.8	4.6 ± 9.6
$(\overline{k}_{\mathrm{eff}})_{ZZZX}$	-6.6 ± 21.5	-3.5 ± 45.7	-5.4 ± 16.6
$(\overline{k}_{\mathrm{eff}})_{ZZZY}$	7.4 ± 23.3	-12.6 ± 45.8	3.4 ± 17.8
$(\overline{k}_{\mathrm{eff}})_{XXYY}$	0.4 ± 1.6	-0.5 ± 8.5	0.4 ± 1.5
$(\overline{k}_{\mathrm{eff}})_{XXZZ}$	0.2 ± 1.6	-0.5 ± 9.1	0.2 ± 1.6
$(\overline{k}_{\mathrm{eff}})_{YYZZ}$	0.6 ± 1.6	-0.3 ± 9.1	0.5 ± 1.6
$(\overline{k}_{\mathrm{eff}})_{XXYZ}$	-3.6 ± 5.7	16.2 ± 25.0	-2.7 ± 5.5
$(\overline{k}_{\mathrm{eff}})_{YYXZ}$	4.7 ± 7.2	7.5 ± 17.2	5.0 ± 6.6
$(\overline{k}_{\mathrm{eff}})_{ZZXY}$	-4.0 ± 6.5	-0.4 ± 2.1	-0.7 ± 1.9

TABLE II: Coefficient values (2σ) from the 2012, 2002, and combined datasets, with all other coefficients vanishing.

bility distribution $p_k = p_k((\overline{k}_{\mathrm{eff}})_{JKLM})$ that is a function of the 15 independent components of $(\overline{k}_{\mathrm{eff}})_{JKLM}$. The p_k are assumed to be gaussian with means μ_k and standard deviations σ_k. The global probability distribution $P = P((\overline{k}_{\mathrm{eff}})_{JKLM})$ of interest is then the product of the individual p_k, taking the form

$$ P = P_0 \exp\left[-\sum_{k=1}^{9} \frac{(\tilde{D}_k - \mu_k)^2}{2\sigma_k^2} \right]. \qquad (7) $$

In this expression, P_0 is an arbitrary normalization. The predicted signal $\mu_k = \mu_k((\overline{k}_{\mathrm{eff}})_{JKLM})$ for the kth amplitude is determined from Eqs. (5) and (6), and the variance σ_k^2 includes all statistical and systematic errors.

An independent measurement of any one chosen component of $(\overline{k}_{\mathrm{eff}})_{JKLM}$ can in principle be obtained by integrating the global probability distribution P over all other components. The result is a distribution involving the chosen component with a single mean and standard deviation, which constitute the estimated component measurement and its error. However, the 2012 dataset alone contains only nine signal components, which is insufficient to constrain independently each of the 15 degrees of freedom in $(\overline{k}_{\mathrm{eff}})_{JKLM}$. Following standard practice in the field [3], we can obtain maximum-sensitivity constraints on each component of $(\overline{k}_{\mathrm{eff}})_{JKLM}$ in turn by integrating the global probability distribution with the other 14 degrees of freedom set to zero. The resulting measurements and 2σ errors on each independent component of $(\overline{k}_{\mathrm{eff}})_{JKLM}$ are displayed in the first two columns of Table II. Note that the first column reveals our choice for the 15 independent components of $(\overline{k}_{\mathrm{eff}})_{JKLM}$. Note also that the sensitivity of the apparatus to the coefficients $(\overline{k}_{\mathrm{eff}})_{JKLM}$ can be crudely estimated as the ratio

of the thermal-noise force at the location of the probe (~ 10 fN) to the scale ($\sim 10\ \mu\mathrm{N/m}^2$) of the amplitudes in the Fourier series (6), multiplied by a suppression factor of order 10^{-2} because the dominant contribution to the noncentral force in a parallel-plate geometry arises from edge effects [29]. This estimate matches the size of the values in the second column of Table II.

The third column of Table II displays the values for the coefficients $(\overline{k}_{\mathrm{eff}})_{JKLM}$ obtained from a comparable analysis of the 2002 dataset. These 2002 results are about a factor of five less sensitive than the 2012 data, a feature that can be traced to the larger average gap between the source and detector masses and the smaller source-mass amplitude in the 2002 experiment. The final column of Table II presents the measured values of each independent component taken in turn that are obtained from analyzing the combined datasets.

The contents of Table II represent the first measurements of noncentral inverse-quartic corrections to Newton gravity and hence of quadratic curvature couplings violating local Lorentz invariance. The inverse-quartic dependence implies the corrections are perturbative at squared distances greater than the coefficient values. For example, the perturbative effects at the apparatus scale are roughly comparable to the Newton force, while on the macroscopic scale of the laboratory the attained constraints exclude noncentral forces at about parts in ten million. An alternative perspective can be obtained by comparing the length dimension associated with the coefficients $(\overline{k}_{\mathrm{eff}})_{JKLM}$ to the various scales set by the Compton wavelengths of elementary particles. The experiment here probes modifications governed to within about an order of magnitude of the scale of the neutrino Compton wavelength. Effects at the scales of Compton wavelengths of other particles would be smaller, reflecting the possibility that comparatively large 'countershaded' Lorentz violation remains a viable possibility [30].

The results reported here set a benchmark for future efforts. For example, upgrading the apparatus used by improving the test-mass and shield flatness could reduce the average gap by a factor of two, and refining the test-mass metrology could reduce the uncertainty in the average gap by a factor of four. Simulations suggest these improvements would increase the overall sensitivity by more than an order of magnitude in the absence of new systematics. With several months of run time, the statistical error bars could be reduced by about another order of magnitude. Moreover, other experimental groups also have the capability of improving substantially over the results in the present work [5]. For example, the HUST experiment has recently reported sensitivities to the coefficients $(\overline{k}_{\mathrm{eff}})_{JKLM}$ surpassing those reported here [29]. Overall, the prospects for improved future short-range searches for Lorentz violation are excellent.

[1] V.A. Kostelecký and S. Samuel, Phys. Rev. D **39**, 683 (1989); V.A. Kostelecký and R. Potting, Nucl. Phys. B **359**, 545 (1991); Phys. Rev. D **51**, 3923 (1995).

[2] For reviews see, for example, J. Murata and S. Tanaka, arXiv:1408.3588; J. Jaeckel and A. Ringwald, Ann. Rev. Nucl. Part. Sci. **60**, 405 (2010); E.G. Adelberger, J.H. Gundlach, B.R. Heckel, S. Hoedl, and S. Schlamminger, Prog. Part. Nucl. Phys. **62**, 102 (2009); E. Fischbach and C. Talmadge, *The Search for Non-Newtonian Gravity*, Springer-Verlag, 1999.

[3] V.A. Kostelecký and N. Russell, *Data Tables for Lorentz and CPT Violation*, 2015 edition, arXiv:0801.0287v8.

[4] C.M. Will, Liv. Rev. Rel. **17**, 4 (2014).

[5] Q.G. Bailey, V.A. Kostelecký, and R. Xu, Phys. Rev. D **91**, 022006 (2015).

[6] V.A. Kostelecký, Phys. Rev. D **69**, 105009 (2004).

[7] D. Colladay and V.A. Kostelecký, Phys. Rev. D **55**, 6760 (1997); Phys. Rev. D **58**, 116002 (1998).

[8] J.C. Long, H.W. Chan, A.B. Churnside, E.A. Gulbis, M.C.M. Varney, and J.C. Price, arXiv:hep-ph/0210004.

[9] J.C. Long, H.W. Chan, A.B. Churnside, E.A. Gulbis, M.C.M. Varney, and J.C. Price, Nature **421**, 922 (2003).

[10] H. Yan, E.A. Housworth, H.O. Meyer, G. Visser, E. Weisman, and J.C. Long, Class. Quant. Grav. **31**, 205007 (2014).

[11] J.B.R. Battat, J.F. Chandler, and C.W. Stubbs, Phys. Rev. Lett. **99**, 241103 (2007).

[12] H. Müller, S.-w. Chiow, S. Herrmann, S. Chu, and K.-Y. Chung, Phys. Rev. Lett. **100**, 031101 (2008).

[13] K.-Y. Chung, S.-w. Chiow, S. Herrmann, S. Chu, and H. Müller, Phys. Rev. D **80**, 016002 (2009).

[14] D. Bennett, V. Skavysh, and J. Long, in V.A. Kostelecký, ed., *CPT and Lorentz Symmetry V*, World Scientific, Singapore 2011.

[15] L. Iorio, Class. Quant. Grav. **29**, 175007 (2012).

[16] Q.G. Bailey, R.D. Everett, and J.M. Overduin, Phys. Rev. D **88**, 102001 (2013).

[17] L. Shao, Phys. Rev. Lett. **112**, 111103 (2014); Phys. Rev. D **90**, 122009 (2014).

[18] Q.G. Bailey and V.A. Kostelecký, Phys. Rev. D **74**, 045001 (2006).

[19] C.D. Hoyle, D.J. Kapner, B.R. Heckel, E.G. Adelberger, J.H. Gundlach, U. Schmidt, and H.E. Swanson, Phys. Rev. D **70**, 042004 (2004); D.J. Kapner, T.S. Cook, E.G. Adelberger, J.H. Gundlach, B.R. Heckel, C.D. Hoyle, and H.E. Swanson, Phys. Rev. Lett. **98**, 021101 (2007).

[20] L.C. Tu, S.-G. Guan, J. Luo, C.-G. Shao, and L.-X. Liu, Phys. Rev. Lett. **98** , 201101 (2007); S.-Q. Yang, B.-F. Zhan, Q.-L. Wang, C.-G. Shao, L.C. Tu, W.-H. Tan, and J. Luo, Phys. Rev. Lett. **108**, 081101 (2012).

[21] J. Murata *et al.*, High Energy News **32**, 233 (2014).

[22] J.K. Hoskins, R.D. Newman, R. Spero, and J. Schultz, Phys. Rev. D **32**, 3084 (1985).

[23] R.S. Decca, D. Lopez, H.B. Chan, E. Fischbach, D.E. Krause and C.R. Jamell, Phys. Rev. Lett. **94**, 240401 (2005); Y.-J. Chen, W.K. Tham, D.E. Krause, D. Lopez, E. Fischbach, and R.S. Decca arXiv:1410.7267.

[24] J. Chiaverini, S.J. Smullin, A.A. Geraci, D.M. Weld, and A. Kapitulnik, Phys. Rev. Lett. **90**, 151101 (2003); S.J. Smullin, A.A. Geraci, D.M. Weld, J. Chiaverini, S.P. Holmes, and A. Kapitulnik, Phys. Rev. D **72**, 122001 (2005); A.A. Geraci, S.J. Smullin, D.M. Weld, J. Chiaverini, and A. Kapitulnik, Phys. Rev. D **78**, 022002 (2008).

[25] A.A. Geraci, S.B. Papp, and J. Kitching, Phys. Rev. Lett. **105**, 101101 (2010).

[26] F. Sorrentino, Q. Bodart, L. Cacciapuoti, Y.-H. Lien, M. Prevedelli, G. Rosi, L. Salvi, and G.M. Tino, Phys. Rev. A **89**, 023607 (2014).

[27] E.G. Adelberger, B.R. Heckel, S.A. Hoedl, C.D. Hoyle, D.J. Kapner, and A. Upadhye, Phys. Rev. Lett. **98**, 131104 (2007).

[28] R. Bluhm, V.A. Kostelecký, C.D. Lane, and N. Russell, Phys. Rev. D **68**, 125008 (2003); Phys. Rev. Lett. **88**, 090801 (2002); V.A. Kostelecký and M. Mewes, Phys. Rev. D **66**, 056005 (2002).

[29] C.-G. Shao, Y.-J. Tan, W.-H. Tan, S.-Q. Yang, J. Luo, and M.E. Tobar, arXiv:1504.03280.

[30] V.A. Kostelecký and J.D. Tasson, Phys. Rev. Lett. **102**, 010402 (2009).